Received: 2 March 2017 | Revised: 31 March 2017 | Accepted: 15 May 2017

DOI: 10.1002/ppap.201700046

FULL PAPER

PLASMA PROCESSES AND POLYMERS

# Pressure as an additional control handle for non-thermal atmospheric plasma processes

**Igor Belov**[1,2] | **Sabine Paulussen**[1] | **Annemie Bogaerts**[2]

[1] Sustainable Materials Management, VITO, Boeretang 200, 2400 Mol, Belgium

[2] PLASMANT, Departement of Chemistry, University of Antwerp, B-2610 Wilrijk-Antwerp, Belgium

**Correspondence**
Igor Belov, Sustainable Materials Management, VITO, Boeretang 200, 2400 Mol, Belgium.
Email: igor.belov@vito.be

**Funding information**
Seventh Framework Programme, Grant number: Grant Agreement № 606889 (RAPID – Reactive Atmospheric Plasma processIng – Education Network)

$O_2$ and $CO_2$ Dielectric Barrier Discharges (DBD) were studied at elevated (i.e., above atmospheric) pressure regimes (1–3.5 bar). It was demonstrated that these operational conditions significantly influence both the discharge dynamics and the process efficiencies of $O_2$ and $CO_2$ discharges. For the case of the $O_2$ DBD, the pressure rise results in the amplification of the discharge current, the appearance of emission lines of the metal electrode material (Fe, Cr, Ni) in the optical emission spectrum and the formation of a granular film of the erosion products (10–300 nm iron oxide nanoparticles) on the reactor walls. Somewhat similar behavior was observed also for the $CO_2$ DBD. The discharge current, the relative intensity of the CO Angstrom band measured by Optical Emission Spectroscopy (OES) and the $CO_2$ conversion rates could be stimulated to some extent by the rise in pressure. The optimal conditions for the $O_2$ DBD ($P = 2$ bar) and the $CO_2$ DBD ($P = 1.5$ bar) are demonstrated. It can be argued that the dynamics of the microdischarges (MD) define the underlying process of this behavior. It could be demonstrated that the pressure increase stimulates the formation of more intensive but fewer MDs. In this way, the operating pressure can represent an additional tool to manipulate the properties of the MDs in a DBD, and as a result also the discharge performance.

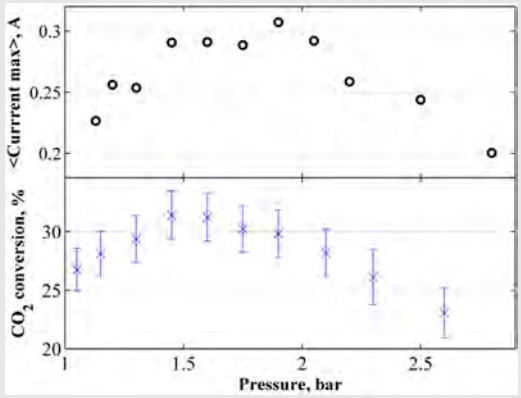


**KEYWORDS**
carbon dioxide, DBD, microdischarge, nanoparticles

## 1 | INTRODUCTION

Plasma reactors are used for a wide range of processes including gas conversion, material synthesis, and surface treatment. The promising technological and economical aspects of non-thermal atmospheric pressure technology in these areas have recently gained a lot of interest.[1–5] However, the control and tuning of Atmospheric Pressure Plasma (APP) systems is not trivial. The plasma chemistry is often governed by plasma parameters which cannot be directly determined by the external settings. For instance, in the specific case of Dielectric Barrier Discharge (DBD) reactors, the plasma is composed of numerous filaments which are known to define the plasma chemistry.[6] The number of these filaments and their properties can, however, not be controlled externally, for instance by the applied

  

voltage.[7] Usually the power input, gas mixture, flow rate, reactor geometry, and excitation type are the parameters used for APP process tuning.[8,9] The power input is considered the main variable that determines the efficiency of the gas conversion.[8,9] In the case of material synthesis applications of APP, it was reported that the gas flow often influences the production rate[10–12] and even morphology of the synthesized product.[13–15] Yet, a better understanding of the underlying principles and dependences is necessary to design an efficient and optimized process.

In this paper, the effect of pressure, and more in particular overpressure, on the material synthesis process in an $O_2$ DBD, and on the conversion reactions in a $CO_2$ DBD, is being studied. Typically, discharge gaps between 0.5 and 3 mm and flow rates in the range of 0.1–10 Standard Liter per Minute (SLM) are applied in laboratory scale APP reactors. Besides, analysis systems such as Gas Chromatographs (GC), Scanning Mobility Particle Sizers (SMPS), Condensation Particle Counters (CPS), or collection filters are often installed in-line with the discharge. Simple engineering estimations suggest that the pressure drop can reach 0.1–4 bar for systems operated at flow rates between 0.1 and 10 SLM. Yet, this phenomenon is not addressed in literature and this type of conditions is referred to as "atmospheric." Often gas flow levels are identified as controlling parameters, but perhaps the increasing pressure drop at increasing gas flows is the actual underlying reason for the differences that can be observed. In this work, we want to assess the impact of increasing pressure on the outcome of APP processes.

The effect of pressure variations between 1 and 3 bar on process efficiency was mainly studied for the production of ozone[16–20] – the most industrialized application of DBD reactors.[21] In recent works, Yuan et al. and Seok et al. demonstrated the existence of an optimal pressure for the ozone synthesis at 1.4 bar for air-fed[20] and 1.5–2 bar for oxygen-fed[19] systems. Furthermore, studies on nanosecond pulsed Surface Dielectric Barrier Discharge (SDBD) development at pressures between 1 and 6 bar in air give evidence for changing discharge dynamics with increasing pressure.[22,23] It was also demonstrated that overpressure can influence plasma-assisted ignition systems[24] as well as the vibrational distribution function in pure $N_2$ discharges.[25]

In this paper, the influence of the operating pressure will be investigated for DBD systems operated in $O_2$ and $CO_2$ at pressures between 1 and 3.5 bar. First, the DBD operating with pure $O_2$ will be used to deposit iron oxide nanoparticles on the reactor walls through etching of the central electrode, while the deposition rate of the nanopowder is measured. Secondly, the efficiency of carbon dioxide dissociation is evaluated in the $CO_2$ DBD. In both cases, the effect of the pressure increase on the discharge behavior and on their performance indicators is evaluated.

## 2 | EXPERIMENTAL SECTION

### 2.1 | Configuration

The experimental setup of the DBD configuration under investigation is schematically shown in Figure 1. A discharge gap of 0.5 mm is obtained between two concentric cylinders, that is, a grounded stainless steel central electrode (outer diameter 25 mm) and a dielectric tube (26 mm inner diameter, 29 mm outer diameter) made of borosilicate glass. A stainless steel mesh is wrapped at the outside of the dielectric tube, acting as an outer electrode and at the same time defining the length of the plasma discharge (215 mm). The inner electrode is grounded while the outer electrode is connected to a power supply with a maximum peak-to-peak voltage of 40 kV, while the excitation frequency was set at 40 kHz (AFS G10S-V generator, AFS GT-30 transformer). The outer electrode arrangement is cooled with deionized water with a controlled conductivity of less than 0.5 $\mu S \cdot m$. This way, local overheating of the reactor and parasitic discharges on the sharp edges of the mesh are prevented. The operating pressure is set within the range of 1–3.5 bar via a pressure gauge and a control valve.

### 2.2 | Power and OES measurement

The applied voltage and the total current are measured by a high voltage probe (Tektronics P6015A) and a Rogowski-type current meter (Pearson Model 4100, 35 MHz), respectively. Due to the design of the reactor it was not possible to introduce an external measuring capacitor in the electrical circuit of the reactor.

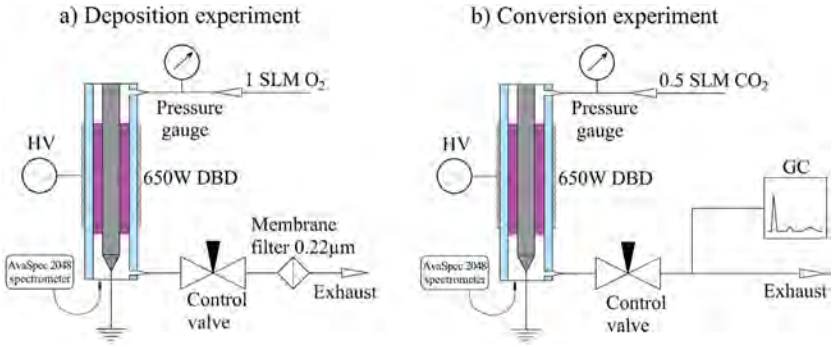


**FIGURE 1** Experimental setup of the tubular Dielectric Barrier Discharge reactor used for (a) nanomaterial production in $O_2$ and (b) gas conversion in $CO_2$

The process is monitored by a 25 MHz PicoScope 2205 digital oscilloscope. Due to the design of the reactor it was not possible to introduce an external measuring capacitor in the electrical circuit of the reactor. The energy input in the discharge is controlled by setting the power of the generator and calculating the corresponding input power value (Equation 1):

$$P_{\text{Input}} = \frac{1}{T}\int_0^T I(t)U(t)dt \quad (1)$$

where $T$ is the period of the AC, and $I(t)$ and $U(t)$ are the measured current and applied voltage signals, respectively.

A survey fiber spectrometer (Avantes, AvaSpec 2048, 180–750 nm range, not shown on Figure 1) with 2.3 nm resolution is used for monitoring the process, collecting light through a 6 mm collimating lens. The lens was pointed on the discharge gap through an optical window (90% transmittance in the 320–600 nm range) installed downstream of the reactor parallel to the electrode axis.

## 2.3 | Deposition experiment

In our previous work we demonstrated that the DBD operated in oxygen containing plasmas gives rise to strong erosion of the metal electrode surface and redeposition of the etched material in the form of a granular metal oxide nanoparticle film on the reactor walls.[26] In the current paper, we study the effect of the operating pressure on the deposit production. The material is collected from the inner surface of the dielectric tube (where it is mostly deposited) in the form of a nanopowder and weighted. The production rate is evaluated via dividing this value by the reaction time (120 min). A membrane filter (Millipore GPWP 02500; diameter, 25 mm; pore size, 0.22 μm) is installed in-line with the reactor to qualitatively demonstrate the presence of the produced nanoparticles downstream of the discharge. An $O_2$ flow rate of 1 SLM and a discharge power of 650W (corresponding to 9.89 eV/molec. specific energy input) are applied in this set of experiments.

## 2.4 | Conversion experiment

Dissociation of $CO_2$ (Equation 2) is taking place in the $CO_2$ DBD:

$$CO_2 \rightarrow CO + 0.5\,O_2, \Delta H = 2.9\,\text{eV/molecule} \quad (2)$$

The gaseous products of the reaction are analysed by a gas chromatograph (Trace-GC, Interscience), equipped with a Thermal Conductivity (TCD) detector. The conversion of $CO_2$ is calculated by comparing the peak area of $CO_2$ in the gas chromatogram before and after plasma exposure (Equation 3):

$$CO_2\ \text{Conversion}\ (\%) = [1 - \frac{\text{moles}\ CO_{2,\ \text{Plasma ON}}}{\text{moles}\ CO_{2,\ \text{Plasma OFF}}}] \times 100\% \quad (3)$$

The $CO_2$ conversion rate obtained at pressures between 1 and 2.5 bar is measured while keeping the power input constant, to demonstrate the influence of the operating pressure on the process efficiency. A $CO_2$ flow rate of 0.5 SLM and a discharge power of 650W (corresponding to 19.78 eV/molec. specific energy input) are applied in this set of experiments.

# 3 | RESULTS

## 3.1 | $O_2$ DBD and its production rate of nanopowder

The effect of pressure elevation on the oxygen discharge can be associated with a modification of the current waveform, as demonstrated in Figure 2. An increase of the discharge current in the positive half-cycle (HC) can be clearly distinguished. An asymmetric current waveform of the $O_2$ DBD with respect to the positive and negative HCs of the applied voltage (described in our previous works[26,27]) can be observed in the whole pressure range investigated (1–3.5 bar).

The dynamics of the discharge current in the positive half-cycle of the $O_2$ DBD upon increasing pressure are presented in Figure 3. Here we introduce the Average Current Maximum (ACM) value. This is the mean amplitude of the current pulse that is calculated via subtracting the sinusoidal component from the measured current waveform. In this way, one can derive the rise of the ACM associated with the pressure increase. Interestingly, the maximum of this value is observed at around 2 bar. A further pressure increase results in the drop of the ACM value. The broad error bars in Figure 3 (especially at P ~ 2 bar) highlight the increase of the presence of the high amplitude pulses (that can be also seen in Figure 2)

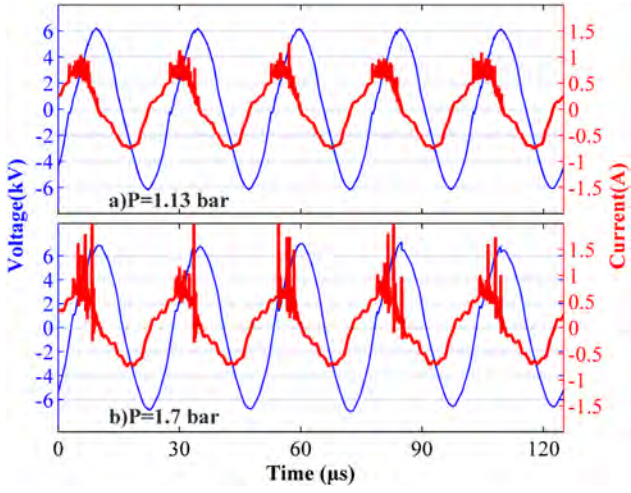


**FIGURE 2** Electrical signal of the $O_2$ DBD at (a) 1.13 and (b) 1.7 bar pressure; Discharge power: 650 W; gas flow rate: 1 SLM

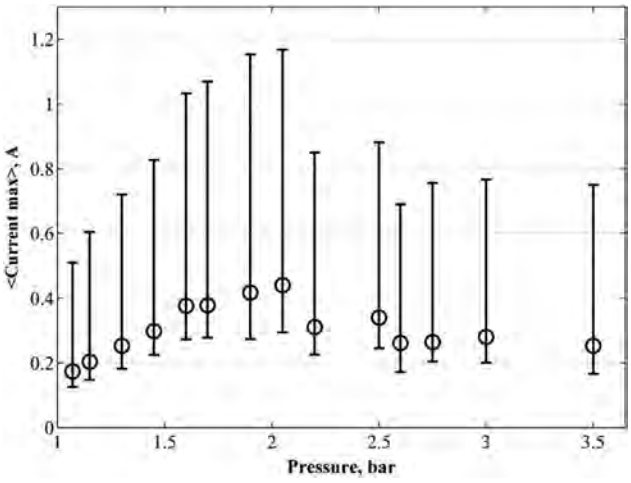


**FIGURE 3** Discharge current, represented by the Average Current Pulse (ACM), in the positive HC of the $O_2$ DBD upon increasing pressure

in the discharge current. In addition to that, visual inspection of the $O_2$ DBD (cf. Figure 4) suggests that more sparse and bright filaments are observed in the $O_2$ DBD at higher pressure.


**FIGURE 4** Images of 1 SLM $O_2$ DBD (exposure time 1/25 s) at (a) $P = 1.3$ bar, (b) $P = 2.1$ bar

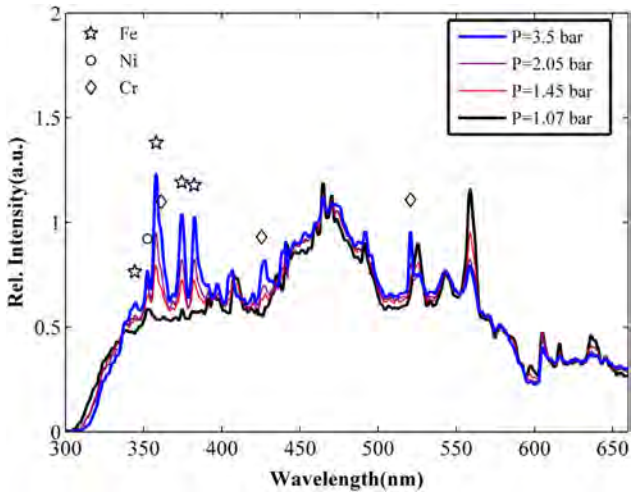


**FIGURE 5** Optical signals of the $O_2$ DBD at various pressures normalized at 459.2 nm

Another effect of the pressure elevation can be noted via Optical Emission Spectroscopy (OES). The $O_2$ DBD emission spectrum normalized at 459.2 nm (maximum of the continuum component in the range 300–650 nm) is presented in Figure 5. The emission lines of the central stainless steel electrode material (Fe, Cr, Ni in the range 340–440 nm) are not observed below $P = 1.45$ bar, but they are becoming brighter with a further pressure increase above 1.45 bar. That effect is also demonstrated in Figure 6, where the relative intensity of the 358.1 nm line (the brightest Fe line in the measured spectrum) grows with increasing pressure.

In our previous paper we found that nanoparticles composed of Fe, O, and C (with the trace presence of the other stainless steel alloy compounds) are formed in the $O_2$ and $CO_2$ DBDs, and that they are deposited on the reactor walls.[26] Here, we extend the analysis by the collection of

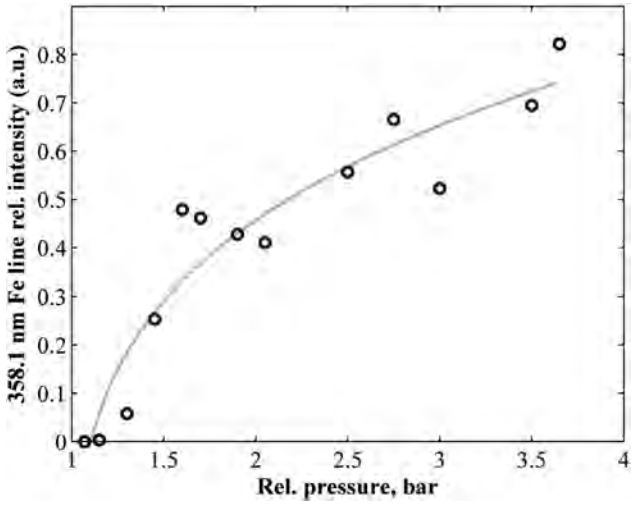


**FIGURE 6** OES intensity of the 358.1 nm Fe line obtained in $O_2$ DBDs upon increasing pressure

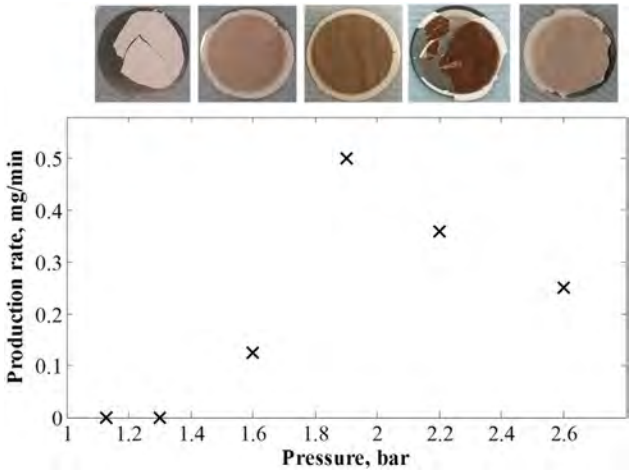


**FIGURE 7** Production rate of nanopowder deposits on the reactor walls in the $O_2$ DBD, and pictures of the 0.22 μm membrane filters installed downstream the reactor after 2 h of operation, at the corresponding pressure regimes

powders through a membrane filter installed downstream of the reactor, in order to qualitatively evaluate the presence of particles guided by the gas flow in the exhaust. In Figure 7 it is demonstrated that the amount of nanopowder collected from the reactor walls highly depends on the operating pressure. Interestingly, at near-atmospheric conditions ($P = 1.13$ and 1.3 bar) almost no particles were found on the reactor walls nor on the filter. The highest powder production rate is observed at a pressure of 1.9 bar, followed by a drop upon higher pressures. Figure 7 also illustrates the qualitative correlation between the powder collected from the reactor walls and the deposits on the membrane filters. The higher production rate corresponds to the thicker (i.e., darker) layer on the filter, while no deposition in the discharge zone results in clean (i.e., white) filter.

A comparison between the ACM and the production rate of the coating is presented in Figure 8. Both parameters behave in a rather similar way upon increasing pressure with a maximum value being reached around 2 bar, followed by a decrease at higher pressures.

## 3.2 | $CO_2$ DBD and its conversion efficiency

An increase of the operating pressure also gives rise to modification of a $CO_2$ DBD. Spectra of the $CO_2$ DBD, normalized at 337.1 nm (the brightest $CO_2$ line that has no large overlap with the CO lines), are shown in Figure 9. The emission spectrum of the filamentary $CO_2$ plasma consists of the highly overlapped Fox system $CO_2/CO_2^+$ lines ($CO_2$[Fox] in the figure) in the range of 300–420 nm, the CO third positive band (280–360 nm), CO Angstrom bands (CO[A] in the figure) in the range between 450 and 700 nm, and a continuum part with a maximum at about 450 nm.[28–31] Similarly to the $O_2$ DBD, the electrode material lines can be observed. Remarkably, an increasing pressure results in a rise of the relative intensity of the CO(A) lines, as can be seen in Figure 9.

Upon pressure rise, an analogous behavior of the increasing discharge current in the positive HC is observed and the current waveform transforms accordingly, similar to that of the $O_2$ DBD (cf. Figure 2). The ACM values of the $CO_2$ DBD also rise with increasing pressure, similar to the $O_2$ DBD (compare Figures 8 and 10). However, further increasing the pressure above 2 bar results again in a drop of the mean current pulse amplitude. Visual inspection of the $CO_2$ discharges also suggests brighter and sparser filaments formed at higher pressures (cf. Figure 11). Interestingly, the $CO_2$ conversion peaks at a pressure of 1.5 bar, while a further increase of the pressure results in a drop of the dissociation rate. As the discharge power is kept constant, the operation at

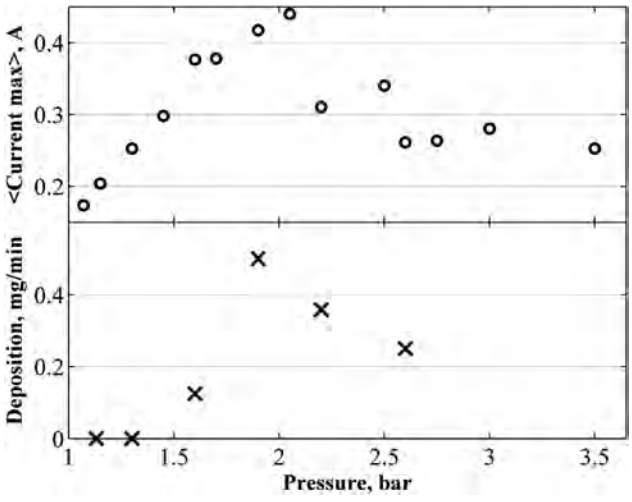


**FIGURE 8** Average current pulse in the positive HC of the $O_2$ DBD (top) and production rate of the collected powder (bottom) as a function of pressure

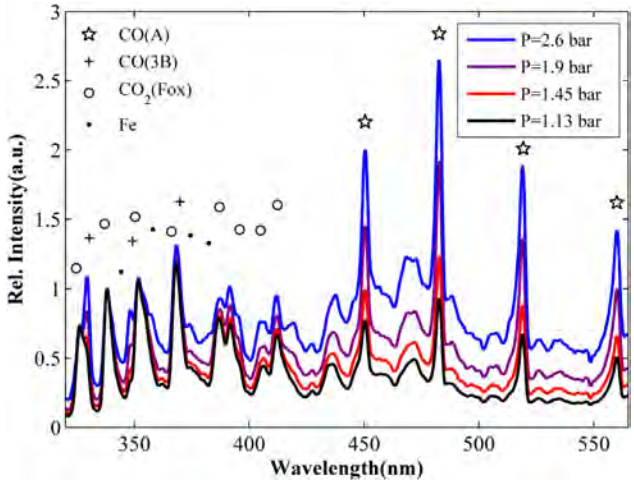


**FIGURE 9** Measured optical signals (normalized at 337.1 nm) of the $CO_2$ DBD at various pressures

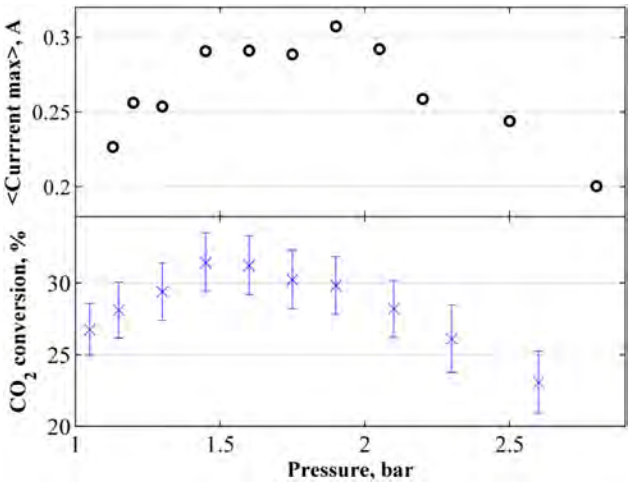


**FIGURE 10** Average current pulse amplitude of the $CO_2$ DBD in the positive HC (top) and $CO_2$ conversion rate (bottom), as a function of pressure. Discharge power: 650 W; $CO_2$ flow rate: 0.5 SLM

1.5 bar results in a higher energy efficiency of the process (4.8% at 1.5 bar vs. 3.5% at atmospheric pressure, when compared to the standard enthalpy of the $CO_2$ decomposition reaction, cf. Equation 2).

## 4 | DISCUSSION

### 4.1 | How can pressure stimulate the microdischarge current in the $O_2$ and $CO_2$ DBDs?

Based on the results shown in the previous sections, we can assume that a pressure increase induces a higher current through a single microdischarge ($I_{MD}$), while the number of the MDs decreases at the same time. This statement can be supported by the following observations:

1. The relative intensity of the metal electrode material lines (such as Fe, Cr, and Ni) and CO(A) bands in the optical emission spectra of the $O_2$ and $CO_2$ DBDs, respectively, rises almost linearly with increasing pressure (cf. Figures 5 and 9);
2. Visual inspection of the $O_2$ and $CO_2$ DBDs suggests that sparser and brighter filaments are formed at higher pressure (cf. Figures 4 and 11);
3. The ACM value rises with increasing pressure, having a maximum around a pressure of 2 bar (cf. Figures 3 and 10 (top), which can be correlated with the decrease of the number of the MDs;

The process variations might be explained by the high electronegativity of the $O_2$ and the products of $CO_2$ dissociation, the decrease of the mean free path at elevated pressures. Because of the latter, the mean electron energy

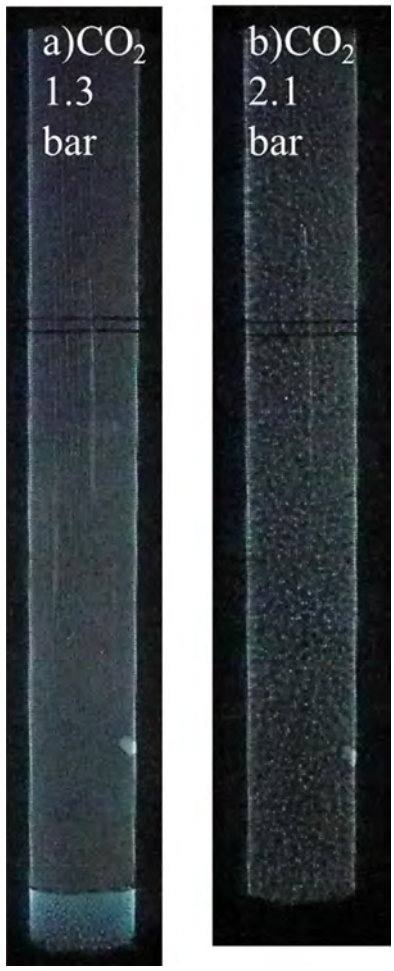


**FIGURE 11** Images of 0.5 SLM $CO_2$ DBD (exposure time 1/25 s) at (a) $P = 1.3$ bar, (b) $P = 2.1$ bar

drops, while the number of collision rises. Such conditions favor electron attachment processes (with low energy thresholds), while ionization reactions (with high energy threshold) become less frequent. This will in turn lead to volume depletion of the electrons and consequently to less frequent ignition of MDs. Thus, charge transfer would be realized through fewer channels, thereby increasing the current passing through a single MD. This hypothesis is backed up by Audier et al., who observed sparser and brighter filaments, tending to ignite repeatedly at the same locations (thus utilizing the strong channels of the extinguished filaments), when the oxygen content was increased in an $N_2$—$O_2$ surface DBD.[32] Similarly Höft et al. associated higher discharge current maxima, a larger MD radius and longer ignition delays with higher $O_2$ concentrations in a single-filament DBD configuration.[33,34]

The decrease of the ACM value toward higher pressure regimes ($P > 2$ bar) might be attributed to the decrease of the overall number of the microdischarges. Indeed, due to the large discharge area, several filaments might be ignited at the same time, causing overlap in the current measurements. In this way, the ACM presents the integrated value of the

microdischarge current and the number of MDs occurring simultaneously. Accordingly, initially (at $P < 2$ bar) the increase of the current is accompanied with a minor drop in the number of MDs. A further pressure rise (at $P > 2$ bar) will significantly decrease the number of filaments, while the current through a single MD will presumably keep increasing. In this way, the increase of the ACM is followed by a drop after $P \sim 2$ bar (cf. Figures 3, 8, and 10). However, as it was stated before, precise information about the properties of the MDs can not be obtained in our system, thus further investigation of the pressure influence on $O_2$ or $CO_2$ discharges should be carried out with a single filament DBD set-up.

## 4.2 | How can pressure stimulate deposition of nanopowder in the $O_2$ DBD?

The oxidation of the metal electrode in oxygen containing DBDs was already reported elsewhere.[19,26,27,35] Our initial observation regarding the nanoparticle production in $O_2$ and $CO_2$ DBD systems was that deposition rates increase at higher flow rates and in higher power regimes. For instance, we observed full coverage of the dielectric tube with powder deposits after 2–5 h at a discharge power of 600W and with a 1 SLM $CO_2$ flow, while it took more than 10 h to obtain the same effect at a $CO_2$ flow of 0.1 SLM.[27] However, as the pressure drop might be significantly different when varying the flow from 0.1 to 1 SLM, the operating pressure (rather than flow rate) might be the parameter determining that process.

Based on the observations reported above, we depict our understanding of the deposition process in Figure 12. First, the MDs evaporate metal from the electrode surface due to the localization of the current transfer (and thus heat transfer) through a narrow ($d \sim 100$–$1000$ μm) filament channel.[12] In this way, the metal vapor is transferred to the gas phase, and thus, Fe, Cr, and Ni lines can be observed in the optical emission spectra. Nucleation, aggregation, agglomeration, and subsequently an increase in particle size occurs in the MD. As a result, nanoparticles ranging in size between 10 and 300 nm are deposited on the surface of the dielectric tube facing the discharge.[26] The deposition on the reactor walls might be attributed to thermophoretic forces ($F_{th}$).[36] Due to thermophoresis, transfer of nanoparticles to the cooler regions can be induced and is guided by the temperature gradient inside the discharge gap, $F_{th} \sim -\nabla T_{gas}$.[37] In the set-ups shown in Figure 1, the dielectric tube is externally cooled ($T_{cool} \sim 20$ °C), while the gas temperature in the DBD can be 100–300 °C higher (not measured in our study, but taken from the literature).[38,39] This temperature gradient could lead to the condensation of nanoparticles on the reactor walls and the formation of a granular film layer with a thickness of about 10 μm.

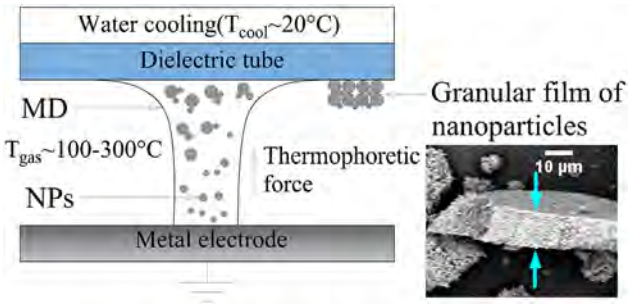


**FIGURE 12** Scheme of the nanoparticle production process in an $O_2/CO_2$ DBD, and SEM image showing the cross section of the granular deposit

As can be seen in Figure 7, solid deposits were not found at pressures close to atmospheric ($P = 1.13$ bar, $P = 1.3$ bar). Comparing Figures 5–7 one might conclude that evaporation only starts when the ACM reaches a value of approximately 0.25 A (at $P > 1.45$ bar). Indeed, at near-atmospheric conditions ($P = 1.13 \ldots 1.3$ bar) the particles were neither collected on the reactor walls nor on the downstream filter, while the emission lines of the electrode material (Fe, Cr, Ni) were not observed in the emission spectrum. It can be argued that with the modulation of pressure (and thus, the MD properties) one can control the power density delivered to the metal surface. As stated before, the change of the gas mixture and the operating pressure can influence the MD parameters, such as current pulse amplitude, duration, and diameter.[33,34] A threshold value of the power density delivered to the metal surface via charge transfer, needed for the electrode vaporization, might be assumed, that can be reached by increasing the MD current via pressure elevation. For further insight in the process, we would require precise information regarding the single MDs, such as the discharge current amplitude, filament radius, and pulse duration. Those parameters define the heat transfer to the electrode surface, thus determining whether or not surface vaporization can occur.[40] These data might be collected in a single filament DBD reactor configuration[33,34,41] and can enable more accurate tuning of the process.

In a number of works, an eroded material from the electrodes in an APP system is deposited as a nanomaterial product, but most often only the influence of the flow rate is demonstrated.[10–15] As stated before, 0.5–1.5 mm gaps or even capillary-sized tubes are commonly used in the discharge design, while the analysis systems are often installed downstream the reactor. Thus, flow variations in such conditions can result in a pressure drop that might also influence the discharge properties. The flow rate indeed plays a substantial role in the development of the material synthesis process, but the findings presented in this paper allow us to suggest that the pressure should also be considered as a control parameter. In this way, pressure regulation will present an additional tuning handle for developing an APP process.

### 4.3 | How can a pressure increase stimulate $CO_2$ conversion?

The explanation for the facilitation of $CO_2$ conversion at increasing pressure is similar to the reasoning behind the increased powder deposition in $O_2$ discharges in similar regimes. The higher discharge current can be associated with a higher electron concentration ($n_e \sim I_{MD}$), and thus, with more frequent electron impact reactions, resulting in higher $CO_2$ decomposition rates. The observations that a higher discharge current is beneficial for the $CO_2$ conversion in a DBD were reported before.[27,35,42] However, the maxima of the $CO_2$ dissociation rate and the mean discharge current values occur at different pressures, as observed in Figure 10. A higher pressure results in a rise of the MD current, but also in a decrease of the number of MDs. Thus, the contact time of the $CO_2$ gas with the filaments will also drop, negatively affecting the conversion.[9] Another reason of the observed decrease of the dissociation rate might be that the $CO_2$ recombination becomes more prominent with increasing pressure.[43]

## 5 | CONCLUSION

In this work we demonstrated that variations in the operating pressure between 1 and 3 bar have a prominent influence on the MD behavior in $O_2$ and $CO_2$ DBD and consequently also on the efficiencies of these systems used for various processes.

A change in the current waveforms, more specifically an amplification of the discharge current in the positive HC, was noted for both the $O_2$ and $CO_2$ DBDs. Furthermore, emission lines of the metal electrode material (Fe, Cr, Ni) appeared in the spectrum of the $O_2$ DBD above $P = 1.45$ bar and they became brighter with further pressure increase. Moreover, solid products in the $O_2$ DBD (i.e., a granular film of the iron oxide nanoparticles) were found only when the pressure was higher than 1.45 bar, while the growth rate had a maximum at $P = 1.9$ bar.

For the $CO_2$ DBD, we observed that the relative intensity of the CO(A) band in the emission spectrum was proportional to the pressure. The $CO_2$ conversion rate reached a maximum value in the $CO_2$ discharge at $P = 1.5$ bar. It was argued that the pressure increase again induces a rise of the discharge current through a single MD and a simultaneous decrease in the number of filaments, thus defining the maximum efficiency of the APP processes.

We can conclude that pressure regulation in APPs might be seen as an additional control handle for the process. Not only it allows to tune the discharge current of the single MDs (and possibly the underlying plasma chemistry) but it also triggers additional effects, such as metal evaporation in the $O_2$ or $CO_2$ DBDs and the $CO_2$ conversion efficiency. These findings are of interest for material synthesis applications and plasma-based $CO_2$ conversion.

## ACKNOWLEDGMENTS

The research leading to these results has received funding from the European Union Seventh Framework Programme (FP7-PEOPLE-2013-ITN) under Grant Agreement № 606889 (RAPID – Reactive Atmospheric Plasma processIng – eDucation network).

## REFERENCES

[1] A. Fridman, *Plasma Chemistry*, Cambridge University Press, New York **2008**.

[2] A. Bogaerts, T. Kozak, K. van Laer, R. Snoeckx, *Farad. Discuss.* **2015**, *183*, 217.

[3] R. Snoeckx, A. Rabinovich, D. Dobrynin, A. Bogaerts, A. Fridman, *Plasma Process. Polym.* **2017**. http://doi.org/10.1002/ppap.201600115

[4] H.-H. Kim, Y. Teramoto, A. Ogata, H. Takagi, T. Nanba, *Plasma Chem. Plasma Process.* **2016**, *36*, 45.

[5] D. Mariotti, T. Belmonte, J. Benedikt, T. Velusamy, G. Jain, V. Švrček, *Plasma Process. Polym.* **2016**, *13*, 70.

[6] P. Bruggeman, R. Brandenburg, *J. Phys. D: Appl. Phys* **2013**, *46*, 464001.

[7] V. G. Samoilovich, V. I. Gibalov, K. V. Kozlov, *Physical Chemistry of the Barrier Discharge* (2 ed.), Deutscher Verlag für Schweisstechnik, Düsseldorf **1997**.

[8] S. Paulussen, B. Verheyde, X. Tu, C. De Bie, T. Marterns, D. Petrovic, A. Boagaerts, B. Sels, *Plasma Sources Sci. Technol.* **2010**, *19*, 034015.

[9] R. Aerts, W. Somers, A. Bogaerts, *ChemSusChem* **2015**, *8*, 702.

[10] J. Gruenwald, K. Fricke, M. Fröhlich, M. Polak, *Plasma Process. Polym.* **2016**, *13*, 946.

[11] J. Gruenwald, K. Fricke, M. Fröhlich, J. F. Kolb, M. Polak, *Plasma Process. Polym.* **2016**, *13*, 766.

[12] J. P. Borra, N. Jidenko, J. Hou, A. Weber, *J. Aerosol Sci.* **2015**, *79*, 109.

[13] D. Mariotti, A. C. Bose, K. Ostrikov, *IEEE Transac. Plasma Sci.* **2009**, *37*, 1027.

[14] J. Fang, L. Schlag, S.-C. Park, T. Stauden, J. Pezoldt, P. Schaaf, H. O. Jacobs, *Adv. Mater.* **2016**, *28*, 1770.

[15] B. Arumugam Chandra, S. Yoshiki, M. Davide, S. Takeshi, T. Kazuo, K. Naoto, *Nanotechnology* **2006**, *17*, 5976.

[16] A. A. Garamoon, F. F. Elakshar, A. M. Nossair, E. F. Kotp, *Plasma Sources Sci. Technol.* **2002**, *11*, 254.

[17] F. Tanaka, T. Iwaishi, T. Sakugawa, H. Akiyama, *2011 IEEE Pulsed Power Conference* **2011**, 1570. http://doi.org/10.1109/PPC.2011.6191684

[18] S. Boonduang, S. Limsuwan, W. Kongsri, P. Limsuwan, *Procedia Eng.* **2012**, *32*, 936.

[19] D. C. Seok, H. Y. Jeong, Y. H. Jung, T. Lho, *Ozone: Sci. Eng.* **2015**, *37*, 221.

[20] D. Yuan, Z. Wang, C. Ding, Y. He, R. Whiddon, K. Cen, *J. Phys. D: Appl. Phys*. **2016**, *49*, 455203.

[21] U. Kogelschatz, *J. Phys. D: Appl. Phys*. **2017**, *50*, 051001.

[22] S. A. Stepanyan, A. Y. Starikovskiy, N. A. Popov, S. M. Starikovskaia, *Plasma Sources Sci. Technol*. **2014**, *23*, 045003.

[23] S. A. Shcherbanev, S. A. Stepanyan, N. A. Popov, S. M. Starikovskaia, *Philos. Transac. R. Soc. A: Math. Phys. Eng. Sci*. **2015**, *373*, 20140342.

[24] S. V. Pancheshnyi, D. A. Lacoste, A. Bourdon, C. O. Laux, *IEEE Transac. Plasma Sci*. **2006**, *34*, 2478.

[25] P. Čermák, J. Varga, P. Macko, V. Martišovitš, and P. Veis, *28th ICPIG* Prague, Czech RepubliF **2007**.

[26] I. Belov, J. Vanneste, M. Aghaee, S. Paulussen, A. Bogaerts, *Plasma Process. Polym*. **2017**, *3*, 1600065.

[27] I. Belov, S. Paulussen, A. Boagaerts, *Plasma Sources Sci. Technol*. **2016**, *25*, 015023.

[28] G. W. Fox, O. S. Duffendack, E. F. Barker, *Proc. Natl. Acad. Sci. USA* **1927**, *13*, 302.

[29] T. Silva, N. Britun, T. Godfroid, R. Snyders, *Plasma Sources Sci. Technol*. **2014**, *23*, 025009.

[30] F. Brehmer, *PhD Thesis Thesis*, Technical University of Eindhoven, **2015**.

[31] T. Oh, *MSc Thesis Thesis*, University of Illinois at Urbana-Champaign, **2013**.

[32] P. Audier, H. Rabat, A. Leroy, D. Hong, *Plasma Sources Sci. Technol*. **2014**, *23*, 065045.

[33] H. Höft, M. Kettlitz, T. Hoder, K. D. Weltmann, R. Brandenburg, *J. Phys. D: Appl. Phys*. **2013**, *46*, 095202.

[34] H. Höft, M. Kettlitz, K. D. Weltmann, R. Brandenburg, *J. Phys. D: Appl. Phys*. **2014**, *47*, 455202.

[35] R. Li, Q. Tang, S. Yin, T. Sato, *Appl. Phys. Lett*. **2007**, *90*, 131502.

[36] E. Thimsen, P. Biswas, *AIChE J*. **2007**, *53*, 1727.

[37] K. De Bleecker, A. Bogaerts, W. Goedheer, *Phys. Rev. E* **2005**, *71*, 066405.

[38] A. Ozkan, T. Dufour, T. Silva, N. Britun, R. Snyders, A. Bogaerts, F. Reniers, *Plasma Sources Sci. Technol*. **2016**, *25*, 025013.

[39] F. Brehmer, S. Welzel, B. L. M. Klarenaar, H. J. v. d. Meiden, M. C. M. v. d. Sanden, R. Engeln, *J. Phys. D: Appl. Phys*. **2015**, *48*, 155201.

[40] B. Jean-Pascal, *J. Phys. D: Appl. Phys*. **2006**, *39*, R19.

[41] T. Hoder, R. Brandenburg, R. Basner, D. Weltmann, K. V. Kozlov, H.-E. Wagner, *J. Phys. D: Appl. Phys*. **2010**, *43*, 124009.

[42] A. Ozkan, T. Dufour, T. Silva, N. Britun, R. Snyders, F. Reniers, A. Bogaerts, *Plasma Sources Sci. Technol*. **2016**, *25*, 055005.

[43] A. Berthelot, A. Bogaerts, *J. Phys. Chem. C* **2017**, *121*, 8236.

**How to cite this article:** Belov I, Paulussen S, Bogaerts A. Pressure as an additional control handle for non-thermal atmospheric plasma processes. *Plasma Process Polym*. 2017;14:e1700046. https://doi.org/10.1002/ppap.201700046